ARTICLES

A Quantum Chemistry Study of the Cl Atom Reaction with Formaldehyde

Margret Gruber-Stadler,[†,‡] Max Mühlhäuser,[†] Stig R. Sellevåg,[§] and Claus J. Nielsen*[,‡]

Studiengang Umwelt-, Verfahrens- und Biotechnik, Management Center Innsbruck Internationale Fachhochschulgesellschaft mbH, Egger-Lienz-Strasse 120, A-6020 Innsbruck, Austria, Centre for Theoretical and Computational Chemistry, Department of Chemistry, University of Oslo, P.O. Box 1033, Blindern 0315 Oslo, Norway, and SINTEF Energy Research, NO-7465 Trondheim, Norway

Received: July 10, 2007; In Final Form: October 8, 2007

The elementary vapor-phase reaction between Cl atoms and HCHO has been studied by ab initio methods. Calculations at the MP2, MP3, MP4(SDTQ), CCSD, CCSD(T), and MRD-CI levels of theory show that the reaction is characterized by a low electronic barrier; excluding the effects of spin−orbit splitting in Cl, our best estimate at the MRD-CI/aug-cc-pVTZ//RHF-RCCSD(T)/aug-cc-pVTZ level of theory predicts a Born−Oppenheimer barrier height of 0.7 kJ mol^{-1}. The energies of the lowest six electronic states as resulting from MRD-CI calculations are presented at discrete points along the reaction path, and two avoided crossings are found in the transition state region. The spin−orbit splitting in Cl is also calculated along the reaction path; it is not negligible in the transition state region and is found to increase the barrier by only 1.4 kJ mol^{-1} at the RCCSD(T)/aug-cc-pVTZ transition state geometry. The minimum energy path of the reaction connects an energetically weakly stabilized adduct on the flat potential surface on the reactant side and an energetically strongly stabilized postreaction adduct. The reaction rate coefficient and the kinetic isotope effects were calculated using improved canonical variational theory with small curvature tunneling (ICVT/SCT), and the results were compared to experimental data. The experimental reaction rate coefficient is reproduced within its uncertainty limits by variational transition state theory with interpolated single-point energy corrections (ISPE) at the MP4(SDTQ) level of theory and by conventional transition state theory with interpolated optimized energies (IOE) at the MRD-CI//RCCSD(T) level of theory and interpolated optimized geometries at the RCCSD(T) level of theory on an MP2/aug-cc-pVTZ potential energy surface when employing scaled vibrational frequencies.

1. Introduction

Formaldehyde, HCHO, is among the key compounds in the chemistry of the lower atmosphere. It is omnipresent being produced in the combustion of fossil fuels, in biomass burning, in the photochemical oxidation of methane and other hydrocarbons, and in microbiological processes. HCHO is the single largest source of H_2 in the atmosphere, it is a sink for radicals, and it plays a significant role as a source of HO_x radicals throughout the atmosphere.

The kinetics of the Cl + HCHO reaction have been studied at room temperature by the relative rate technique using Fourier transform infrared spectroscopy,[1] by infrared chemiluminescence following laser-induced generation of Cl atoms,[2] by discharge flow-mass spectrometry,[3] by discharge flow-electron paramagnetic resonance,[4] and by flash photolysis-resonance fluorescence.[5] Two temperature studies, both using flash photolysis-resonance fluorescence, have been reported.[6,7] The recommended reaction rate coefficient is $k_T = 8.2 \times 10^{-11} \exp(-34/T)$ and $k_{298} = 7.3 \times 10^{-11}$ cm^3 molecule^{-1} s^{-1},[8] that is, virtually without temperature dependence. Experimental D, ^{13}C, and ^{18}O kinetic isotope effects in the Cl atom reaction with formaldehyde at room temperature are also available.[9,10]

We have previously reported results from ab initio calculations (MP2) of the Cl + HCHO reaction including conventional transition state calculations of the reaction rate coefficient and the kinetic isotope effects;[9] conventional transition state theory (TST) did not reproduce the observed kinetic isotope effects in a satisfactory manner. More recently the Cl + HCHO reaction was investigated by time-resolved infrared emission spectroscopy supported by density functional theory (DFT) and single-point energy CCSD(T) calculations.[11] As already shown in our previous computational study,[9] the B3LYP/DFT calculations are not adequate in describing the reaction. In the present study we extend the previous ab initio calculations on the reaction of formaldehyde with chlorine to a high level of theory to elucidate the barrier of the "almost barrierless" reaction. We also extend the previous TST model to variational transition state theory with the aim of calculating reaction rate coefficients in better agreement with experiment and improve the fundamental understanding of the origin to kinetic isotope effects.

* Author to whom correspondence should be addressed. E-mail: c.j.nielsen@kjemi.uio.no.

† Management Center Innsbruck Internationale Fachhochschulgesellschaft mbH.

‡ University of Oslo.

§ SINTEF Energy Research.

10.1021/jp0753833 CCC: $40.75
Published on Web 12/11/2007

2. Computational Methods

2.1. Electronic Structure Calculations. The ground-state potential energy surface (PES) of the HCHO + Cl reaction system was investigated at the MP2,[12] MP3,[13] MP4(SDTQ),[14,15] and CCSD[16−19] levels of theory with the Gaussian 03 program.[20] Unrestricted wave functions were used to describe open-shell systems and bond breaking processes; singlet ground state structures were calculated using restricted wave functions. Additional RHF-RCCSD(T)[21] coupled cluster geometry optimizations were carried out employing the MOLPRO 2002.6 program package[22] in which both open- and closed-shell systems are described by the RHF-RCCSD(T) model.[23−25] We have chosen the partially spin-restricted RHF-RCCSD(T) over the spin-unrestricted RHF-UCCSD(T) model because spin-unrestricted RHF-UCCSD(T) caused severe convergence problems for the investigated system. The core electrons were kept frozen in the calculations. Dunning's correlation-consistent cc-pVXZ (X = D, T)[26,27] and aug-cc-pVXZ (X = D, T, Q) basis sets[26−28] were employed in all calculations. The optimized structures were tested by vibrational analyses to be local minima (Hessian with only positive eigenvalues) and saddle points (Hessian with one negative eigenvalue).

Single-point energies at the MP4(SDTQ)/aug-cc-pVXZ (X = T, Q, 5)[26−30] and CCSD(T)/aug-cc-pVXZ (X = T, Q) levels of theory were calculated for the MP2/aug-cc-pVDZ and MP2/aug-cc-pVTZ stationary points with the Gaussian 03 program. In addition the energies of the ground and electronically excited states of the stationary points, obtained in the MP2/aug-cc-pVXZ (X = D, T) and RHF-RCCSD(T)/aug-cc-pVTZ calculations, were computed using the selecting multireference single- and double-excitation configuration interaction method MRD-CI implemented in the DIESEL program.[31] Additional ground-state and electronically excited-state energies for three nonstationary points along the MP2/aug-cc-pVTZ minimum energy path of reaction (section 2.2) were calculated to give the potential energy curves of the ground state and five energetically low-lying electronic states. In these calculations we employed the aug-cc-pVTZ basis set,[26−28] which is flexible with respect to polarization and electron correlation and is considered to be fairly balanced for the present system. This basis set has proved to give reasonable results in calculations on similar systems.[32−34] In the DIESEL program package the selection of reference configurations can be carried out automatically according to a summation threshold. We have chosen a summation threshold of 0.85, which means that the sum of the squared coefficients of all reference configurations selected for each electronic state is above 0.85. The number of reference configurations for each irreducible representation was in the range between 7 and 22 for the stationary and nonstationary points. The 19 valence electrons of the system were treated as active while keeping the remaining 14 electrons of the inner shells in doubly occupied orbitals (frozen). With this set of reference configurations all single and double excitations in the form of configuration state functions (CSFs) were generated. From this MRD-CI space all configurations with an energy contribution ΔE(Thr) above a given threshold Thr were selected; i.e., the contribution of a configuration larger than this value relative to the energy of the reference set was included in the final wave function. A selection threshold of Thr = 5×10^{-8} hartree was used for the calculation of the states. The effect of configurations that contribute less than Thr = 5×10^{-8} hartree is accounted for in the energy computation, E(MRD-CI), by a perturbative technique.[35,36] The contribution of higher excitations was estimated by applying a generalized Langhoff−Davidson correction formula E(MRD-CI + Q) = E(MRD-CI) − (1 − c_0^2) [E(ref) − E(MRD-CI)]/c_0^2, where c_0^2 is the sum of squared coefficients of the reference species in the total CI wave function and E(ref) is the energy of the reference configurations. In total, we examined 12 low-lying electronically excited doublet states at each stationary and nonstationary point of the system.

The energies of the MP2/aug-cc-pVTZ and MP2/aug-cc-pVQZ geometry-optimized structures as well as the MP4(SDTQ)/aug-cc-pVQZ and MP4(SDTQ)/aug-cc-pV5Z single-point energies of the MP2/aug-cc-pVTZ structures were extrapolated toward the basis-set limit using the extrapolation scheme of Halkier et al.[37]

$$E_{XY}^{\infty} = \frac{X^3 E_X - Y^3 E_Y}{X^3 - Y^3} \quad (1)$$

where E_X is the correlation energy obtained with the highest cardinal number X and E_Y is the correlation energy obtained with cardinal number Y equal to $X - 1$. The cardinal numbers of the aug-cc-pVTZ, aug-cc-pVQZ, and aug-cc-pV5Z basis sets are 3, 4 and 5, respectively. In the following such calculations will be denoted MP2/EB$_{XY}$ and MP4(SDTQ)/EB$_{XY}$//MP2/aug-cc-pVTZ, respectively, with "EB" being short for extrapolated basis.

2.2. Calculation of Reaction Rate Coefficients. The minimum energy path (MEP) connecting reactants and products was computed at the MP2/cc-pVDZ, MP2/aug-cc-pVDZ, and MP2/aug-cc-pVTZ levels of theory using the intrinsic reaction coordinate (IRC) method of Gonzales and Schlegel.[38,39] The IRC calculations were carried out in mass-weighted Cartesian coordinates using a step size of 0.02 u$^{1/2}$ bohr. Calculations of rate coefficients were carried out on the MP2/aug-cc-pVTZ MEP using interpolated variational transition state theory by mapping (IVTST-M)[40] using the sparse grid of geometries, gradients, and Hessians from the ab initio IRC calculations as the input (the ratio between gradients and Hessians was 3:1). The MEP was followed in mass-scaled (scaling mass equal to 1 u) curvilinear coordinates using the RODS algorithm.[41] The electronic energy of the MEP was corrected by the interpolated single-point energy (ISPE) method[42] using the MP4(SDTQ) energies of the reactants, products, saddle point, pre- and postreaction adducts as inputs. In a second procedure, the interpolated optimized energies (IOE) method[43,44] in which the RCCSD(T)/aug-cc-pVTZ geometries and the MRD-CI/aug-cc-pVTZ//RCCSD(T)/aug-cc-pVTZ energies of the reactants, saddle point, and products were used. The electronic energies of the MEP were corrected by the SECKART method in which a single Eckart potential is fitted to the differences between the higher-level MRD-CI/aug-cc-pVTZ//RCCSD(T)/aug-cc-pVTZ and lower-level MP2/aug-cc-pVTZ energies at all stationary points. From this information the ground-state vibrationally adiabatic potential curves, V_a^G, were obtained.

The rate coefficients were calculated over the temperature range of 200−1500 K using improved canonical variational theory (ICVT).[45,46] Semiclassical tunneling corrections have been included using the centrifugal-dominant small-curvature adiabatic ground-state tunneling (SCT) approximation.[46,47] The transmission coefficient also includes the classical adiabatic ground-state (CAG) transmission coefficient[48] that adjusts the quantal corrections for the difference between V_a^G at its maximum and at the CVT transition state. The calculations of the kinetic isotope effects were based on a single reaction path using the methods outlined in refs 41, 49, and 50. The POLYRATE program[51] was used to calculate the rate coefficients.

In the present reaction, the two spin−orbit (SO) states $^2P_{3/2}$ (lowest) and $^2P_{1/2}$ of Cl having degeneracies of 4 and 2, respectively, and separated by 882.3515 cm^{-1} (10.6 kJ mol^{-1})[52] were included in the calculation of the electronic partition function. To estimate the contribution of SO coupling to the potential energy surface of the reaction SO matrix elements were calculated for the stationary points obtained at the MP2/aug-cc-pVTZ and RHF-RCCSD(T)/aug-cc-pVTZ levels of theory using the Breit−Pauli Hamiltonian as implemented in the MOLPRO 2002.6 program package.[53] Wave functions for the SO states were generated using MRCI with reference CASSCF configurations only and the 6-311++G(3df, p) basis set.

The vibrational−rotational partition functions were assumed to be separable, and the rotational partition functions were approximated by their classical limit. The vibrational partition functions were as a standard calculated within the harmonic oscillator approximation for all modes. Alternatively, the force constants of all modes were scaled in the calculations based on the MP2/aug-cc-pVTZ MEP. The scaling factor $c = 0.8975$ applied to the force constants was calculated according to[54]

$$c = \sum(\tilde{\nu}_i^{\text{exp}} \cdot \tilde{\nu}_i^{\text{theo}}) / \sum(\tilde{\nu}_i^{\text{theo}})^2 \qquad (2)$$

where $\tilde{\nu}_i^{\text{exp}}$ are the experimental frequencies of vibration and $\tilde{\nu}_i^{\text{theo}}$ are the theoretically calculated frequencies of vibration for the modes of HCHO, HCO, and HCl.

3. Results

We report results from a detailed computational study of the HCHO + Cl reaction. First, we introduce the minimum energy path and the stationary points in the reaction. Then we present the energies of the stationary points at high levels of theory, elucidating the barrier to the reaction: The electronic energies referred to do not include the effects of the spin−orbit coupling in the Cl atom. We then show how the electronically excited states change during the reaction before turning attention to the spin−orbit coupling in Cl and to the effect that this has on the potential energy surface of the reaction. Finally we address calculation of the reaction rate coefficient and the kinetic isotope effects.

3.1. Stationary Points and Minimum Energy Path of Reaction. The MEP connecting reactants and products was computed using the IRC method.[38,39] Figure 1 shows the potential energy, V_{MEP}, along the IRC calculated at the MP2/cc-pVDZ, MP2/aug-cc-pVDZ, and MP2/aug-cc-pVTZ levels of theory. The improved theoretical description of the reaction system by enlarging the basis set lowers the barrier height and flattens the shape of the potential energy surface. In addition to the saddle point of the hydrogen abstraction reaction, we have located a prereaction van der Waals adduct on the MEP. On the product side of the MEP there is a postreaction van der Waals adduct between HCO and HCl as already reported by Beukes et al.[9] They also reported the existence of a stable adduct between the Cl atom and formaldehyde in which the Cl atom is bonded to the oxygen atom of the carbonyl group. Our calculations confirm the existence of this adduct. We find, however, that it is not situated on the MEP of the reaction.

The stationary points on the MEP of the Cl reaction with HCHO were optimized at several levels of theory. The structures of the adducts and the saddle point are displayed in Figure 2, while the structural parameters obtained at the different levels of theory are listed in Table 1. Structure data for formaldehyde and the products are available in Table S1 (Supporting Information). When comparing the structural results for formaldehyde and the reaction products with the experimental values[55] (Table S1) it is seen that the bond lengths in formaldehyde and hydrochloric acid are calculated within a range of less than ±2.0 pm from the experimental values for all levels of theory in agreement with the established error margins.[56] For the formyl radical the deviations are larger spanning a range between −3.0 pm (C═O bond at the MP3/aug-cc-pVTZ level of theory) and +5.5 pm (C−H bond at the RHF-RCCSD(T)/aug-cc-pVDZ level of theory). Whereas the bond angles of formaldehyde are described in close agreement with experimental data (largest deviation −0.3°), the bond angle of the formyl radical deviates between +4.3° and +5.5° in all calculations. The applied levels of theory thus provide reasonable descriptions of the reactants and products; the aug-cc-pVTZ and aug-cc-pVQZ basis sets perform superior to the aug-cc-pVDZ basis set.

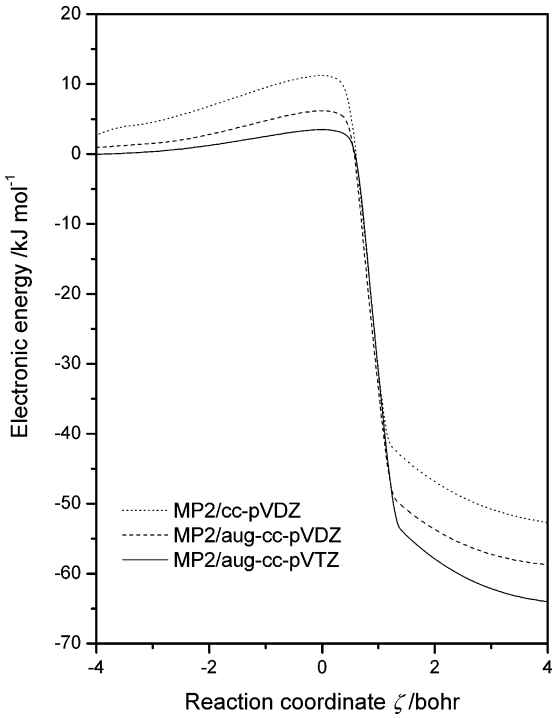

Figure 1. Potential energy along the minimum energy path, V_{MEP}, as resulting from MP2 IRC calculations employing the cc-pVDZ, aug-cc-pVDZ, and aug-cc-pVTZ basis sets.

The structural parameters of the saddle point show noticeable differences at the various levels of theory. The structure becomes more and more reactant-like going from the MP2/aug-cc-pVDZ to the RHF-RCCSD(T)/aug-cc-pVTZ levels of theory. A comparison between the MP2/cc-pVDZ and the MP2/aug-cc-pVDZ results shows that expanding the basis set by diffuse functions shifts the saddle point toward the reactants on the reaction path. This trend is continued when the basis set is enlarged and/or the level of treatment of correlation effects is improved. At the RHF-RCCSD(T)/aug-cc-pVTZ level of theory the H···Cl distance, R_4, and the C···H···Cl angle, α_3, deviate considerably from the other results. An inspection of the potential energy dependency on the C···H···Cl angle shows that an increase of the angle up to 170° raises the electronic energy by only 0.16 kJ mol^{-1}, indicating a very loose character of the transition state.

3.2. Energies of Stationary Points. The energies of the stationary points relevant to the reaction are summarized and compared to previous results in Table 2. The prereaction adduct is stabilized by less than 4 kJ mol^{-1} whereas the energy of the postreaction adduct lies approximately 10 kJ mol^{-1} below the energy of the products. The calculated enthalpies of reaction

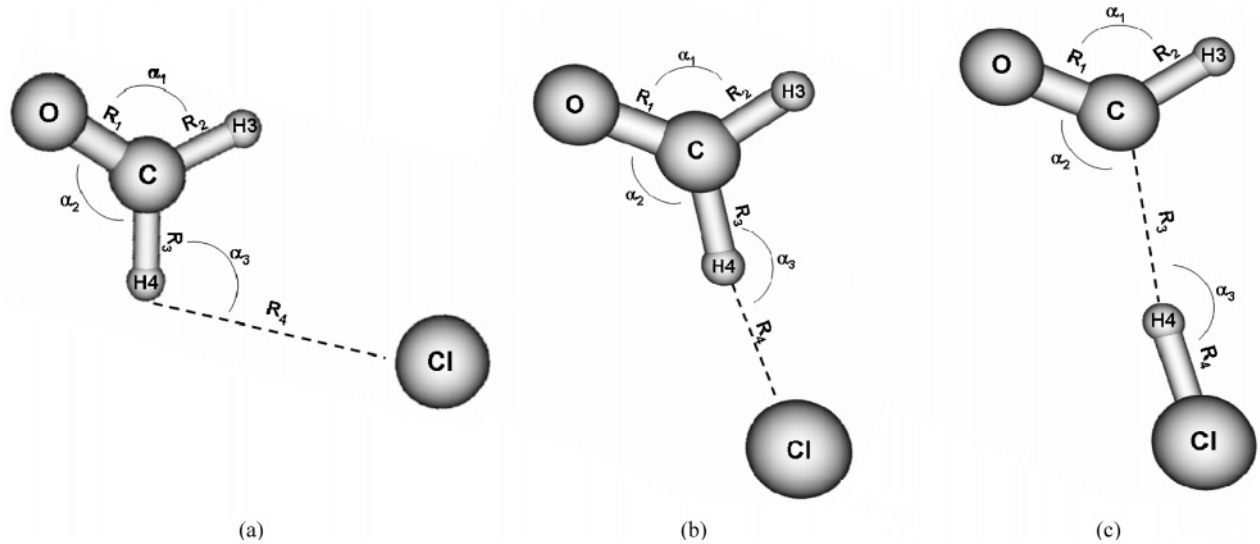

Figure 2. Structures of the (a) prereaction adduct, (b) the saddle point, and (c) the postreaction adduct in the reaction HCHO + Cl → HCO + HCl. The results from different levels of theory are given in Table 1.

are in reasonable agreement with the experimental value;[54] the deviations reflect what can be expected according to previous investigations of the accuracy of ab initio calculated reaction enthalpies.[57] The MP2/aug-cc-pVXZ (X = D, T) reaction enthalpies are in remarkably good agreement with experiment. This may result from some error cancellation between the approximate *N*-electron treatment and the basis-set incompleteness as found by Helgaker and co-workers for atomization energies,[57] or it can be due to the fact that the basis set superposition error (BSSE) and the basis set convergence error are often of opposite signs as pointed out by Dunning.[58] The basis set extrapolation employed at the MP2/aug-cc-pVXZ (X = T, Q) and MP4(SDTQ)/aug-cc-pVXZ//MP2/aug-cc-pVTZ (X = Q, 5) levels of theory yields extrapolated energies less than 1.1 kJ mol^{-1} lower than those obtained with the highest basis set cardinal number, indicating that the results are near the basis set limit of the respective levels of theory.

A challenging issue in the reaction concerns the existence of a barrier and, eventually, its height. An examination of the Born−Oppenheimer barrier height evaluated at the saddle point, $\Delta E^{\ddagger}$, relative to the energies of the reactants reveals that it decreases with the increasing level of theory and that the saddle point energy even becomes negative for geometry optimizations at the RHF-RCCSD(T)/aug-cc-pVDZ level of theory and in single-point energy calculations at the MP4(SDTQ)/aug-cc-pV5Z and CCSD(T) levels of theory; see Table 2. The electronic barrier height is clearly less than the so-called "chemical accuracy" of approximately 4 kJ mol^{-1}, an energy range that—even for small systems—is difficult to address reliably in ab initio calculations. For the loosely bound adducts and the saddle point one may therefore expect the BSSE to be significant. To estimate the magnitude of this effect, the BSSE was approximated by the counterpoise correction scheme of Galano and Alvarez-Idaboy.[59] They proposed an atom by atom scheme where the intermolecular BSSE, associated with the A−B interaction, is obtained by substracting the intramolecular BSSE of the fragments from the intramolecular BSSE of the supermolecule and considering every atom as a fragment in the calculation of all of the intramolecular BSSE. This approach decreases the reported counterpoise overcorrection of the A−B interaction when calculating the BSSE by the conventionally used counterpoise correction scheme of Boys and Bernardi.[60,61] The results, included in Table 2, show that the effect cannot be neglected in the present system—around 1 kJ mol^{-1} for the RHF-RCCSD(T)/aug-cc-pVTZ calculations—but its magnitude is within the range of values reported for several similar systems.[60,62,63] The barrier height of the saddle point as resulting from geometry optimization at the highest level of theory of the present study (RHF-RCCSD(T)/aug-cc-pVTZ) changes from −1.1 to +0.05 kJ mol^{-1} when correcting for the BSSE. Although the basis set superposition error amounts to critical values in the present system considering the barrier height of the reaction, BSSE corrections were not included in the subsequent calculations of reaction rates and kinetic isotope effects because one has to take into account the basis set truncation error, which is of the opposite sign. When comparing the energies at the MP2/aug-cc-pVTZ level of theory and the basis set extrapolated energies, MP2/EB$_{43}$, in Table 2, it can be seen that for the electronic energy of reaction, $\Delta_{rxn}E$, and the adduct on product side, $\Delta E_{post-adduct}$, the basis set truncation error is larger than the BSSE, whereas for the barrier height, $\Delta E^{\ddagger}$, and the electronic energy of the adduct on reactant side, $\Delta E_{pre-adduct}$, the basis set truncation error is in the range of the BSSE.

Another indication of a barrier comes from the results of the single-point energy multireference configuration interaction calculations (MRD-CI); see also section 3.3. Whereas the CCSD(T) single-point energy calculations based on the MP2/aug-cc-pVXZ (X = D, T) geometries result in "negative barrier heights", the MRD-CI calculations give positive barrier heights, an indication that a multireference treatment is necessary to account for the complete configuration interaction along the reaction path. The same is observed for the MRD-CI/aug-cc-pVTZ calculations based on the RHF-RCCSD(T)/aug-cc-pVTZ geometries: The barrier height of −1.1 turns into +0.7 kJ mol^{-1} in the MRD-CI calculation. Comparing the results of our MRD-CI and RCCSD(T) calculations, one has to consider two effects: size inconsistency and spin contamination. Spin contamination and size inconsistency both overestimate the barrier. To avoid the size inconsistency problem in the MRD-CI calculations we did not use isolated reactants and products but largely separated non-interacting reactants and products at a distance of 20 Å in a supermolecular approach. In our RCCSD(T) calculations spin contamination is not a problem because a restricted wave function is used. The RCCSD(T) model does not take into account nondynamical correlation

TABLE 1: Structural Parameters[a] of the Saddle Point, the Prereaction Adduct, and the Postreaction Adduct in the Reaction HCHO + Cl → HCO + HCl[b]

	transition state						adduct on reactant side						adduct on product side					
level of theory	R_1	R_2	R_3	R_4	α_1	α_2	α_3	R_1	R_2	R_3	R_4	α_1	α_2	α_3	R_1	R_2	R_3	R_4	α_1	α_2	α_3
MP2/aug-cc-pVDZ	1.203	1.114	1.153	1.918	124.4	121.6	170.5	1.224	1.112	1.112	3.234	121.8	121.8	104.8	1.194	1.127	2.219	1.299	124.6	123.1	173.6
MP2(full)/cc-pVDZ[9]	1.196	1.118	1.160	1.901	125.1	122.3	170.6								1.190	1.132	2.321	1.293	124.5	129.7	165.8
MP2/aug-cc-pVTZ	1.196	1.102	1.138	1.921	124.3	121.5	168.4	1.213	1.101	1.101	3.234	121.9	121.9	105.1	1.183	1.114	2.197	1.287	125.0	121.9	174.1
MP2/aug-cc-pVQZ	1.194	1.101	1.134	1.946	124.1	121.4	166.4	1.209	1.100	1.100	3.234	121.9	121.9	105.1	1.179	1.113	2.199	1.286	125.0	121.9	174.1
MP3/aug-cc-pVTZ	1.180	1.101	1.160	1.803	125.2	121.4	171.9														
MP4(SDTQ)/aug-cc-pVTZ	1.200	1.107	1.129	2.053	123.8	121.1	165.8														
CCSD/aug-cc-pVTZ	1.190	1.101	1.146	1.884	124.3	121.4	170.6								1.174	1.115	2.349	1.284	125.6	120.8	171.4
RHF−RCCSD(T)/aug-cc-pVDZ	1.213	1.115	1.137	2.087	123.3	121.4	167.4														
RHF−RCCSD(T)/aug-cc-pVTZ	1.208	1.103	1.112	2.344	122.5	121.4	155.9	1.211	1.104	1.104	3.252	121.6	121.6	102.3	1.181	1.118	2.264	1.288	125.2	121.8	172.5

[a] See Figure 1 for definition of distances and angles. [b] Distances (R_x) are given in ångstroms, and bond angles (α_x) in degrees.

because a single-configuration wave function is used as basis for the calculation of the dynamical correlation energy. MRD-CI calculations are based on a multiconfiguration wave function that is able to describe nondynamical correlation like it is present in the HCHO + Cl reaction where the reactants (considered in a supermolecular approach) are threefold degenerate (see next section) due to the SO splitting of the chlorine atom. At the saddle point an avoided crossing can be observed as pointed out in the next section, and spin−orbit coupling is not quenched totally (see section 3.4). Therefore a multiconfigurational treatment of the saddle point is supposedly more accurate than the RCCSD(T) model that uses only a single-configuration wave function. Additionally, RCCSD(T) is not variational, which could lead to energies lower than the exact result for the reactants and/or saddle point. Because of excluding the size inconsistency of the MRD-CI model by applying the supermolecular approach we assume that the energy calculations by the MRD-CI model and consequently the barrier height at the MRD-CI level of theory are more accurate than the results obtained by the RCCSD(T) model.

3.3. Electronically Excited States. Figure 3 shows the potential energy curves of the lowest six electronic states along the minimum energy path of the HCHO + Cl reaction. The electronically excited states were calculated at the MRD-CI level of theory for the stationary points, optimized at the RHF-RCCSD(T)/aug-cc-pVTZ level of theory, and for three additional values of the reaction coordinate ($\zeta = -2.7$, $\zeta = +0.7$, and $\zeta = +1.3$) along the MEP of the reaction obtained from MP2/aug-cc-pVTZ calculations. The geometries of the stationary points correspond to the structures given in Table 1 with reference to Figure 2 and in Table S1. With C_s symmetry throughout the MEP of the reaction, the electronic configuration of the supermolecule is $...(3a'')^2(13a')^2(14a')^1$. Formaldehyde possesses C_{2v} symmetry with an X^1A_1 ground state. In the supermolecule the A_1 and B_1 states of formaldehyde correlate with the A′ irreducible representation of C_s, while A_2 and B_2 states correlate with A″. For the chlorine atom the $^2P_{3/2}$ states correlate with A′, while the $^2P_{1/2}$ state, which is antisymmetric with respect to reflection through the molecular plane, correlates with A″. At the reactant side (isolated HCHO + Cl), the ground state of the supermolecule is threefold degenerate, leading to two A′ states (X^1A_1 of HCHO paired with $^2P_{3/2}$ of Cl) and one A″ state (X^1A_1 of HCHO paired with $^2P_{1/2}$ of Cl). The ground state of the supermolecule is X^2A'.

The lowest excitation of the reactants originates from the n → π^* transition in the C═O group of formaldehyde (corresponding to the 1^3A_2 state of HCHO). It is well-established that this spin-forbidden transition is promoted by spin−orbit interactions through the mixing of the 1^3A_2 and 2^1A_1 (π, π^*) states involving coupling of the R_z component of the SO Hamiltonian.[64] Investigations on the dissociation of formaldehyde show that the 1^3A_2 surface opens—besides the ground-state surface—the channel to H + HCO via S_1-T_1 intersystem crossing.[65,66] Our calculations place the transition at 3.76 eV (363 kJ mol^{-1}, 330 nm), in reasonable agreement with experiments[67,68] and previous theoretical calculations.[69,70] Like the ground state, this energetically lowest excitation is also threefold degenerate, leading to one A′ and two A″ states.

In the entrance channel on the reactant side the degenerate states split. In parallel the Cl atom becomes loosely bound. The $1^2A''$ and $2^2A'$ states originate from a transition of molecular orbitals (MOs) dominated by the p_y and p_z atomic orbitals (AOs) of Cl into the highest occupied molecular orbital (HOMO), which can be characterized by the p_x (Cl) AO with increasing

TABLE 2: Energetics of Stationary Points in the Reaction HCHO + Cl → HCO + HCl Relative to That of the Reactants

computational level	$\Delta_{rxn}E^a$/kJ mol^{-1}	$\Delta_{rxn}H^0$/kJ mol^{-1}	$\Delta E^{\ddagger}$/kJ mol^{-1}	$\Delta V_a^{G\ddagger}$/kJ mol^{-1}	i$\omega^{\ddagger}$/cm^{-1}	$\Delta E_{pre-adduct}$/kJ mol^{-1}	$\Delta E_{post-adduct}$/kJ mol^{-1}
MP2/cc-pVDZ	−42.3	−59.8	11.2	7.9	263.0	−2.3	−54.1
MP2(full)/cc-pVDZ[9]	−43.0		10.7				−54.9
MP2/aug-cc-pVDZ	−46.9	−64.6	6.2	3.5	240.2	−3.6	−59.1
MP2(full)/aug-cc-pVDZ[9]	−48.0		4.4		262.0		−61.2
MP2/cc-pVTZ	−50.3	−68.0	6.0	2.4	205.2	−2.4	−61.3
MP2/aug-cc-pVTZ	−52.7	−70.3	3.5 (7.3)	0.3 (4.1)	197.5	−3.5 (−2.6)	−64.4 (−63.0)
MP2/aug-cc-pVQZ	−56.3	−74.0	3.3	−0.2	174.8	−3.3	−67.4
MP2/EB$_{43}$ (aug-cc-pVTZ/aug-cc-pVQZ)	−57.1		3.8			−3.3	−68.0
MP3/aug-cc-pVTZ	−36.8	−54.8	9.4	1.3	359.0		
MP4(SDTQ)/aug-cc-pVTZ	−47.3	−64.9	0.5	−0.3	230.5		
CCSD/aug-cc-pVTZ	−36.5	−54.6	3.1	−2.2	116.9		−44.9
RHF−RCCSD(T)/cc-pVDZ	−33.9	−51.9	6.7	1.2	142.5		
RHF−RCCSD(T)/aug-cc-pVDZ	−38.5	−56.5	−0.6	−0.04	239.9		
RHF−RCCSD(T)/cc-pVTZ	−40.2	−58.2	1.7	−1.3	73.3		
RHF−RCCSD(T)/aug-cc-pVTZ	−42.7	−60.4	−1.1 (0.05)	−2.3 (−1.1)	104.0	−3.5 (−2.7)	−52.9 (−52.5)
MP4(SDTQ)/aug-cc-pVTZ//MP2/aug-cc-pVDZ	−47.4	−65.1	0.11	−2.6		−3.7	−59.0
CCSD(T)/aug-cc-pVTZ//MP2/aug-cc-pVDZ	−43.2	−61.3	−3.4	−6.1		−4.1	−53.2
MRD−CI/aug-cc-pVTZ//MP2/aug-cc-pVDZ	−37.8	−55.5	4.7	2.0		−2.5	−58.8
MP4(SDTQ)/aug-cc-pVQZ//MP2/aug-cc-pVTZ	−51.4	−68.9	0.05	−3.1		−3.5	−62.2
MP4(SDTQ)/aug-cc-pV5Z//MP2/aug-cc-pVTZ	−53.7	−71.2	−0.15	−3.3			
MP4(SDTQ)/EB$_{54}$//MP2/aug-cc-pVTZ	−54.7	−72.3	−0.32	−3.5			
CCSD(T)/aug-cc-pVTZ//MP2/aug-cc-pVTZ	−43.6	−61.2	−5.2 (−1.4)	−8.4 (−4.6)		−3.6 (−2.7)	−53.7 (−52.4)
CCSD(T)/aug-cc-pVQZ//MP2/aug-cc-pVTZ	−47.5	−65.1	−5.9	−9.0			
MRD−CI/aug-cc-pVTZ//MP2/aug-cc-pVTZ	−54.5	−72.1	0.9	−2.3		−4.6	−61.2
MRD−CI/aug-cc-pVTZ//RHF−RCCSD(T)/aug-cc-pVTZ	−44.2	−62.0	0.7	−0.5		−2.3	−52.5
experimental[54]		−65.3					

[a] $\Delta_{rxn}E$ is the Born−Oppenheimer (electronic) energy of reaction; $\Delta_{rxn}H^0$ is the enthalpy of reaction at 0 K; $\Delta E^{\ddagger}$ is the Born−Oppenheimer barrier height evaluated at the saddle point; $\Delta V_a^{G\ddagger}$ is the ground-state vibrationally adiabatic barrier height evaluated at the saddle point; i$\omega^{\ddagger}$ is the imaginary frequency of the saddle point; $\Delta E_{pre-adduct}$ is the electronic energy of the adduct on reactant side; $\Delta E_{post-adduct}$ is the electronic energy of the adduct on product side. All energies are relative to that of the reactants. Values in parentheses include a counterpoise correction.

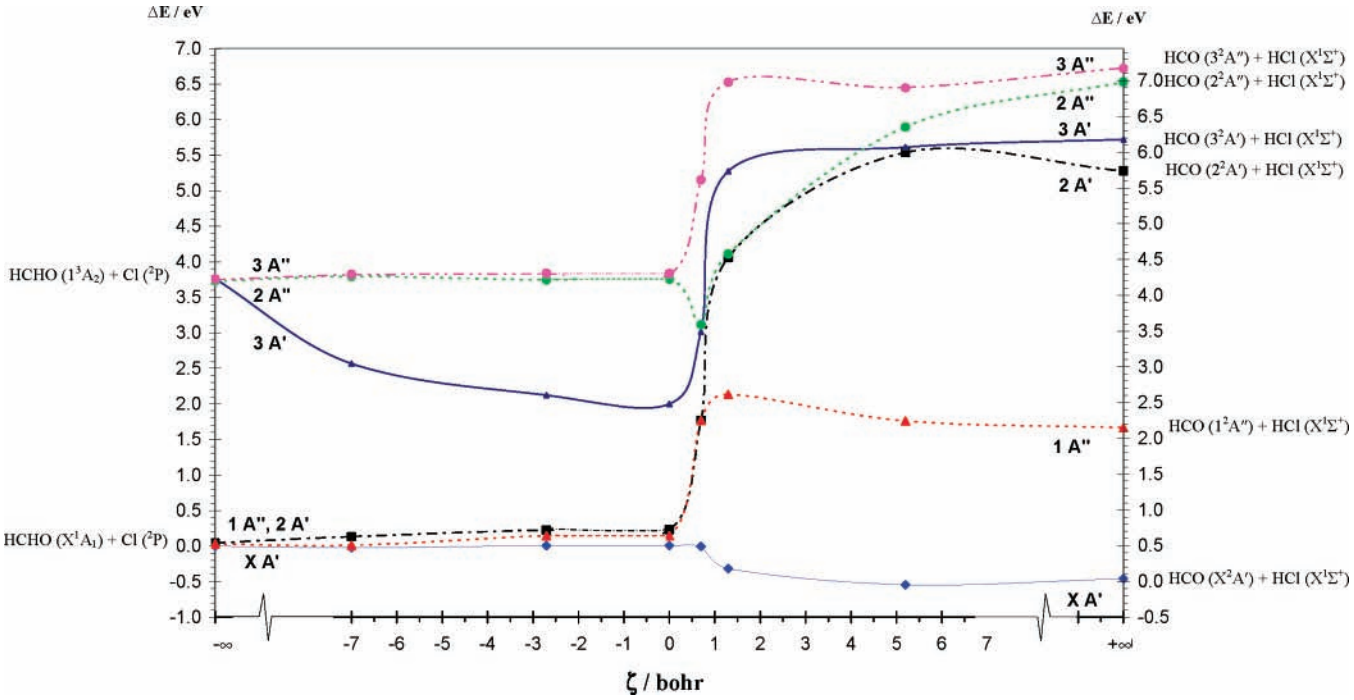

Figure 3. Calculated MRD-CI potential energy curves of the ground state and the lowest five excited states along the reaction path of formaldehyde and chlorine. The vertical excitation energies were computed at RHF-RCCSD(T)/aug-cc-pVTZ geometries at the stationary points and at MP2/aug-cc-pVTZ geometries at the nonstationary points at $\zeta = -2.7$, $\zeta = 0.7$, and $\zeta = 1.3$ applying C_s symmetry for the system. On the reactant side (left-hand side), the excitation energies are given with respect to the reactants; on the right-hand side, the energies can be read with respect to the products.

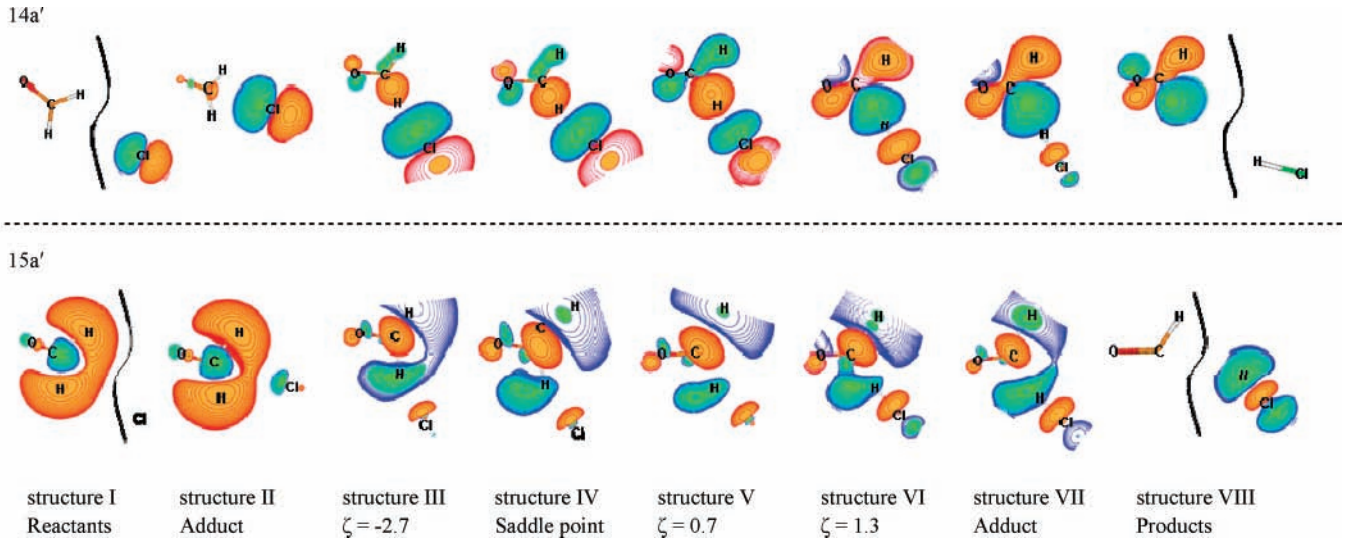

Figure 4. Charge density contours of the HOMO (14a′) and the low-lying virtual orbital 15a′ along the reaction path.

contributions of the sp^2 (C) AO. This is illustrated in Figure 4 where the evolution of the charge density contours of the HOMO (14a′) and the unoccupied orbital 15a′ along the reaction path is displayed. These low-lying states correspond to a rotation of the singly occupied Cl AO around the *y*- and *x*-axes. The two A′ states (rotation around the *y*-axis) separate to avoid a crossing, the energy of the $^2P_{3/2}$ (^2P_x) state is lowered (ground state X^2A'), and the energy of the $^2P_{3/2}$ (^2P_z) state is increased ($2^2A'$). In the entrance channel the $1^2A''$ state is energetically located between X^2A' and $2^2A'$. A similar splitting is found for the two upper A″ states corresponding to an avoided crossing of $2^2A''$ and $3^2A''$. These excitations correspond to an n → π^* transition mixed with a rotation of the singly occupied Cl AO around the *y*-axis. The $3^2A'$ state originates from a $\sigma_{C-H} \rightarrow \sigma_{H-Cl}$ transition. Along the entrance channel the transition decreases in line with the cleavage of the C···H and the formation of the H···Cl bond.

In the region of the saddle point toward the exit channel two avoided crossings can be observed: (i) between $1^2A''$ and $2^2A''$ and (ii) between $2^2A'$ and $3^2A'$. $1^2A''$ in which the Cl AO is rotated around the *x*-axis relative to the ground state correlates with the exit channel leading to HCl ($X^1\Sigma^+$) + HCO ($1^2A''$). The excitation of the formyl radical $1^2A'' \leftarrow X^2A'$ corresponds to an n → π^* transition. The second avoided crossing occurs between the states $2^2A'$ and $3^2A'$. Both states resemble excited HCO ($2^2A'$ and $3^2A'$) and HCl in its ground state ($X^1\Sigma^+$). In the entrance channel the supermolecule with the $^2P_{3/2}$ (^2P_x) state of Cl (X^2A') correlates with the products both being in the ground state. The calculated excitation energies of HCO of 2.12 eV (205 kJ mol^{-1}, 585 nm) ($1^2A'' \leftarrow X^2A'$), 5.73 eV (553 kJ mol^{-1}, 216 nm) ($2^2A' \leftarrow X^2A'$), and 6.18 eV (596 kJ mol^{-1}, 201 nm) ($3^2A' \leftarrow X^2A'$) are in reasonable agreement with experiments[71−73] and prior theoretical calculations.[74]

In the saddle point region where bond-breaking/formation takes place, the electronic energy levels change dramatically. For the saddle point on the RHF-RCCSD(T)/aug-cc-pVTZ surface, MRD-CI calculations place the lowest electronically excited states at 13.3 ($1^2A''$) and 21.4 ($2^2A'$) kJ mol^{-1} above the ground state.

In Figure 4 we present the evolution of charge density contours of the highest occupied valence orbital HOMO (14a′) and the low-lying virtual orbital 15a′ along the reaction path. The lowest unoccupied molecular orbital (LUMO (3a″) is of A″ symmetry and is therefore not included in Figure 4. Structures I and VIII in Figure 4 correspond to the reactants and products, respectively. Structure II corresponds to the weakly bound adduct on the reactant side (Figure 2a), structure IV is the transition state (Figure 2b), and structure VII represents the adduct on the product side (Figure 2c). In addition, we have included three points on the reaction path: $\zeta = -2.7$, $\zeta = +0.7$, and $\zeta = +1.3$.

The existence of a barrier along the reaction path can be understood from qualitative MO considerations. On the reactant side (structure I in Figure 4), the HOMO (14a′) is of lone pair character representing the 3p AO located at the chlorine center. In the product structure (structure VIII in Figure 4) the corresponding MO is the unoccupied 15a′, which again shows lone pair character at the chlorine center. Both occupations lead to A′ states. Consequently we observe an avoided crossing in the saddle point region. While on the reactant (structure I) and product sides (structure VIII) the nature of the MOs is of genuine lone pair 3p AO (Cl) character, it can be seen that at the saddle point (structure IV) the MO 14a′ is represented by an almost equal linear combination of 3p AO (Cl) and sp^2 (C). Furthermore the 2p AO (O) is also involved. The HOMO on the reactant side (structures II and III) again is dominated by 3p AO (Cl) whereas the HOMO on the product side (structures V−VII) shows an increasing influence of the O═C−H part. The finding for MO 15a′ is similar: Going from structures I to VIII the 3p AO (Cl) becomes more important in the linear combination.

3.4. Spin−Orbit Coupling. The spin−orbit coupling in the Cl atom results in a splitting of the Cl atom ground configuration into $^2P_{3/2}$ and $^2P_{1/2}$ states separated by 882.3515 cm^{-1}.[52] This splitting changes during the reaction and should therefore be included in the potential energy function. To estimate the contribution of the SO coupling to the potential energy surface of the reaction system we calculated the energy splitting due to SO coupling at the stationary points and three additional nonstationary points along the MEP. Assuming that SO coupling is only relevant in the reactants' region as found for the Cl + HCl reaction system,[75] the SO coupling will lower the asymptotic potential energy of the reactants by $^1/_3$ of the SO splitting (294 cm^{-1}, 3.5 kJ mol^{-1}). On the MP2/aug-cc-pVTZ MEP the calculations predict the SO coupling to lower the asymptotic potential energy of the reactants by 3.3 kJ mol^{-1}, in good agreement with the a priori assumption of $^1/_3$ of the SO coupling constant of Cl (3.5 kJ mol^{-1}) and previous calculations on similar systems.[75,76] The same SO coupling is found in the prereaction adduct. Figure 5 summarizes the calculated SO coupling as a function of the reaction coordinate. At the reaction coordinate $\zeta = -2.7$ the SO coupling lowers the energy by 2.3 kJ mol^{-1}. At the saddle point there is still a SO coupling of 0.6 kJ mol^{-1} computed. At $\zeta = 0.7$ the SO coupling decreases to 0.12 kJ mol^{-1} and finally vanishes at $\zeta = 1.3$, where the $1^2A''$ state strongly rises in energy.

Starting from the RHF-RCCSD(T) structures the SO coupling results in the same values as for the MP2 structures for the reactants, the pre-, and postreaction adducts as well as the products, but it amounts to a lowering of 1.9 kJ mol^{-1} at the saddle point. The lower excitation energy for the $1^2A''$ and $2^2A'$ states and the larger SO coupling for the higher-level geometry (RHF-RCCSD(T) compared to MP2) can be rationalized in terms of differences in the structure of the saddle point; the nature of the saddle point becomes more reactant-like going from the MP2 to the RHF-RCCSD(T) level of theory.

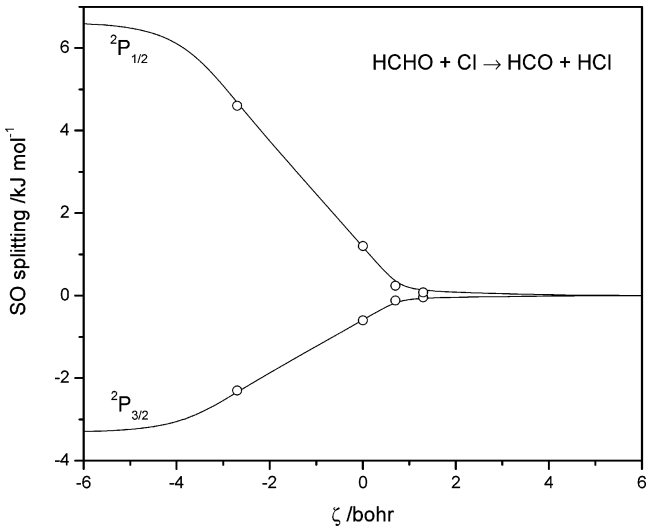

Figure 5. Calculated SO splitting in Cl as a function of the reaction coordinate on the MP2/aug-cc-pVTZ MEP. See text for details on the calculations.

The spin−orbit coupling was considered in the calculation of the rate constants by increasing the electronic barrier height. The excited spin−orbit states were only considered in the electronic partition function of the chlorine atom. Assuming adiabaticity, only the ground-state PES correlates to products; nonadiabatic transitions to low-lying excited SO states in the transition state (TS) region are not considered in our calculations. Therefore the electronic partition function at the TS is set equal to 2.

3.5. Absolute Rate Coefficients. As previously mentioned an improved theoretical description of the reaction system by enlarging the basis set lowers the barrier height and flattens the shape of the potential energy surface. This trend is continued by the dual-level reaction path dynamics leading to a barrier height close to zero. Figure 6 shows the potential energy of the minimum energy path, V_{MEP}, for the reaction and the ground state vibrationally adiabatic potential energy curve, ΔV_a^G, as a function of the reaction coordinate, ζ, calculated at the MP2/aug-cc-pVTZ level of theory. The figure also includes the corresponding curves corrected by the ISPE method using single-point energy corrections from MP4/aug-cc-pVQZ calculations and by the IOE method using geometry corrections at the RCCSD(T)/aug-cc-pVTZ level of theory and energy corrections from MRD-CI/aug-cc-pVTZ//RCCSD(T)/aug-cc-pVTZ calculations. The curves result from an interpolation of 300 ab initio points with gradients and where the Hessians have been computed at 100 of these points. The progressions of the V_{MEP} and ΔV_a^G curves obtained by the IOE method differ significantly from the curves of the MP2 model and the ISPE dual-level method. This behavior results from the difference in the energies of the postreaction adduct and products: At the MRD-CI/aug-cc-pVTZ//RCCSD(T)/aug-cc-pVTZ level of theory, the electronic energies of the postreaction adduct, $\Delta E_{post-adduct}$, and the enthalpy of reaction, $\Delta_{rxn}H^0$, are 11.9 and 8.3 kJ mol^{-1}, respectively, higher than those at the MP2/aug-cc-pVTZ level

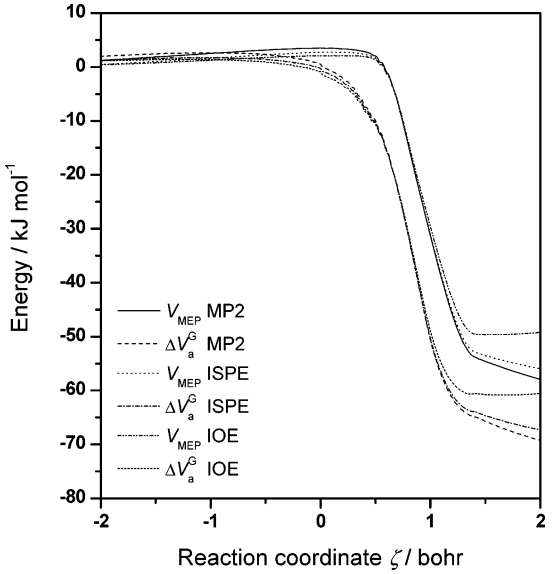

Figure 6. Minimum energy path, V_{MEP}, and vibrationally adiabatic ground-state potential energy curve, ΔV_a^G, as a function of the reaction coordinate, ζ, for the reaction HCHO + Cl → HCO + HCl calculated at the MP2/aug-cc-pVTZ level of theory without and with dual-level reaction path dynamics by interpolated single-point energies (ISPE) and interpolated optimized energies (IOE) corrections. (All values are relative those of the reactants.)

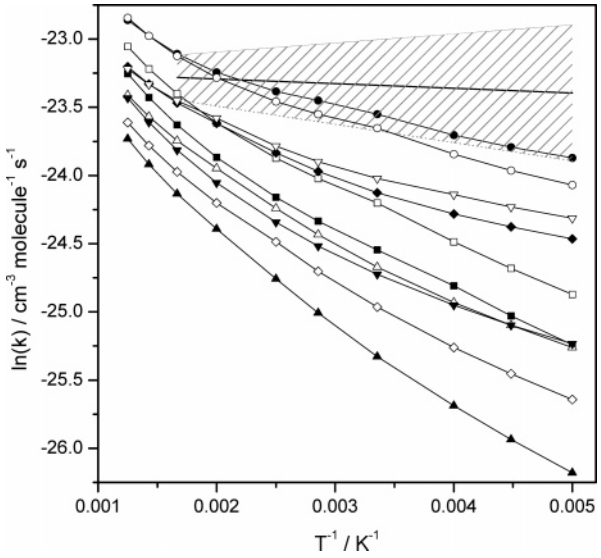

Figure 7. Arrhenius plot of calculated and experimental rate coefficients for the reaction HCHO + Cl → HCO + HCl; (filled upward triangles) ICVT/SCT with MP2/aug-cc-pVTZ data, (open diamonds) ICVT/SCT with ISPE including SO coupling, (open downward triangles) ICVT/SCT with ISPE, (open upward triangles) ICVT/SCT with IOE including spin−orbit (SO) coupling, (filled squares) ICVT/SCT with ISPE including SO coupling and scaled force constants (scaling factor = 0.8975), (open squares) ICVT/SCT with IOE including SO coupling and scaled force constants (scaling factor = 0.8975), (filled diamonds) ICVT/SCT with IOE, (filled downward triangles) TST with MP2/aug-cc-pVTZ data, (filled circles) ICVT/SCT with ISPE and scaled force constants (scaling factor = 0.8975), (open circles) ICVT/SCT with IOE and scaled force constants (scaling factor = 0.8975), (——) Atkinson et al.[8] evaluation of reference data with uncertainty limits.

of theory, each relative to the energy of the reactants. At the MP4/aug-cc-pVQZ//MP2/aug-cc-pVTZ level of theory that is applied in the ISPE calculations, the differences are only +2.2 and +1.4 kJ mol^{-1} for $\Delta E_{post-adduct}$ and $\Delta_{rxn}H^0$, respectively. The generalized normal-mode frequencies of the system as a function of the reaction coordinate are shown in Figure S1 (Supporting information). Not only the CH_2-related modes in formaldehyde are affected during the H abstraction reaction—the symmetric CH_2 stretching mode at 2889 cm^{-1}, the CH_2 scissor mode at 1532 cm^{-1}, and the CH_2 rocking mode at 1263 cm^{-1} but also the C═O stretching mode (1907 cm^{-1}) change its character considerably in the interval $\zeta = 0-1.5$.

Figure 7 shows Arrhenius plots of calculated rate coefficients from different models of the HCHO + Cl reaction. For comparison the figure includes a plot of the recommended rate coefficient including its uncertainty limits. Because SO coupling present in the Cl atom becomes smaller during the reaction it will contribute to the potential energy surface by effectively increasing the barrier height. This was taken into account in the calculation of the rate coefficients. For the IOE method the barrier height for the energy corrections at the MRD-CI/aug-cc-pVTZ//RCCSD(T)/aug-cc-pVTZ level of theory was increased by 1.4 kJ mol^{-1}, which is the net effect of the SO coupling at the RCCSD(T)/aug-cc-pVTZ geometries. In the ISPE model the barrier height was increased by 2.7 kJ mol^{-1} according to the SO coupling calculated for the MP2/aug-cc-pVTZ geometries. The reaction enthalpy and the energy of the postreaction adduct were also corrected for the effect of spin−orbit coupling. This method of accounting for SO coupling in dual-level calculations has proved to give reasonable results for other reaction systems.[76,77] As can be seen from Figure 7, the consideration of SO coupling lowers the rate coefficients significantly compared to the rates obtained by neglecting the effect of SO coupling. For the IOE model the rate coefficients are lowered by about 42% at 298 K and 28% at 500 K; for the ISPE model the values are 63% and 46% at 298 and 500 K, respectively.

The ICVT/SCT results based on the MP2 Hessians significantly underestimate the rate coefficients for the reaction and do not reproduce the temperature dependence correctly. The shortfallen rate coefficients are not surprising because the vibrational frequencies have been calculated within the harmonic oscillator approximation, which is known to overestimate the experimental frequencies. Scaling the force constants of all modes by a factor of 0.8975 results in a considerable increase of the rate constants for both the ISPE and the IOE model. For the ISPE dual-level calculations, scaling of the force constants results in rate coefficients that reproduce the experimental values within the uncertainty limits.

Table 3 lists the calculated rate coefficients of the Cl reaction with formaldehyde obtained from the IOE model, taking into account the effect of SO coupling in comparison to experimental data in the temperature range between 200 and 1500 K. In addition, Table 3 includes the ratio of the reaction rates obtained by conventional transition state theory and improved canonical variational theory, k^{TST}/k^{ICVT}, and the ratio of reaction rates without and with consideration of small curvature tunneling in the calculation, $k^{ICVT}/k^{ICVT/SCT}$ for the IOE and the ISPE models. An analysis of the numbers shows that variational effects are significant in the HCHO + Cl reaction, especially at low temperatures. This effect is more pronounced for the ISPE model. It is slightly lowered for both models when scaling of the frequencies is applied.

Two effects with opposed consequences to the reactions rate coefficients can be observed: (i) The vibrational frequencies calculated within the harmonic oscillator approximation overestimate the experimental frequencies and normally generate too large reaction rates within the TST model, representing the upper bound of the rates. The inclusion of variational effects in the calculation of rate coefficients, but still based on overesti-

TABLE 3: Absolute Reaction Rate Constants, k, in Units of 10^{-11} cm^3 Molecule^{-1} s^{-1} and Ratios of Rate Constants for HCHO + Cl → HCO + HCl[a]

		IOE						ISPE			
		$k^{ICVT/SCT}$		k^{TST}/k^{ICVT}		$k^{ICVT}/k^{ICVT/SCT}$		k^{TST}/k^{ICVT}		$k^{ICVT}/k^{ICVT/SCT}$	
T/K	$k_{experiment}$[8]	unscaled	scaled	unscaled	scaled	unscaled	scaled	unscaled	scaled	unscaled	scaled
200	6.92	1.07	1.58	2.779	2.072	0.972	0.968	4.312	3.462	0.964	0.954
223	7.04	1.26	1.91	2.463	1.790	0.986	0.974	3.497	2.785	0.972	0.963
250	7.16	1.49	2.32	2.190	1.559	0.987	0.978	2.876	2.256	0.981	0.976
298	7.32	1.93	3.09	1.890	1.309	0.990	0.984	2.211	1.841	0.986	0.977
350	7.44	2.45	3.69	1.690	1.236	0.988	0.989	1.811	1.605	0.989	0.985
400	7.53	2.97	4.29	1.549	1.185	0.993	0.993	1.561	1.462	0.991	0.988
500	7.66	3.98	5.55	1.419	1.129	0.995	0.995	1.362	1.285	0.994	0.993
600		4.87	6.9	1.387	1.093	0.998	0.997	1.254	1.184	0.995	0.995
700		5.81	8.3	1.367	1.070	0.998	0.998	1.186	1.122	0.998	0.997
800		6.8	9.7	1.352	1.052	0.999	0.998	1.140	1.079	0.998	0.997
900		7.8	11.2	1.343	1.045	0.999	1.000	1.108	1.054	0.998	0.998
1000		8.9	12.7	1.337	1.056	0.999	0.992	1.083	1.048	0.999	1.000
1500		15.0	20.5	1.313	1.078	1.000	1.000	1.023	1.040	1.000	1.000

[a] The reaction rates are obtained with unscaled vibrational frequencies and with scaling of the force constants by a factor of 0.8975, both within the harmonic approximation. Abbreviations: IOE, interpolated optimized energies; ISPE, interpolated single-point energies; TST, conventional transition state theory; ICVT, improved canonical variational transition state theory; SCT, small-curvature tunneling.

TABLE 4: Kinetic Isotope Effects, $\alpha = k_{light}/k_{heavy}$, in the Reaction of Formaldehyde with Chlorine at 298 K[a]

	ISPE		IOE			
	ICVT/SCT			ICVT/SCT		
isotopologues	unscaled	scaled	TST	unscaled	scaled	experiment
HCHO/DCDO	1.646	1.810	1.367	1.043	1.198	1.302 ± 0.014[9], 1.31 ± 0.01[10], 1.35 ± 0.15[1]
HCHO/HCDO	1.253	1.318	1.128	0.998	1.069	1.201 ± 0.002[10]
H^{12}CHO/H^{13}CHO	0.986	1.005	0.992	0.985	0.997	1.058 ± 0.007[10], 1.07 ± 0.03[9]
H^{13}CHO/DCDO	1.669	1.802	1.379	1.059	1.420	1.217 ± 0.025[9]
HCHO/HCH^{18}O	1.000	1.000	1.011	1.016	1.016	1.08 ± 0.01[10]

[a] The reaction rates are obtained by direct variational transition state theory with interpolated single-point energies (ISPE) and interpolated optimized energies (IOE) dynamics calculations based on electronic structure information at the MP2/aug-cc-pVTZ level of theory as explained in the text. In both models the force constants are scaled by a factor of 0.8975 to correct the vibrational frequencies within the harmonic approximation. KIEs calculated with conventional transition state theory (TST) and improved canonical variational transition state theory with small-curvature tunneling (ICVT/SCT) are compared with experimental measurements.

mated vibrational frequencies, leads to a lowering of the reaction rates. (ii) To account for the deficiency in frequencies the force constants were scaled, presumably leading to a more correct description of the system within the variational transition state theory and consequently to improved reaction rate coefficients. However, the error due to the harmonic approximation depends on temperature and therefore is of minor importance at 200 K but still present. The anharmonic vibrational calculation along the reaction path could supposedly correct for this insufficiency; however, presently these calculations are too expensive at a proper level of theory.

The second parameter accounted for in our calculations employing ICVT is the small curvature tunneling (SCT). The factor analysis in Table 3 shows relatively small contributions of SCT to the rate coefficients that are more pronounced in the lower-temperature range.

3.6. Kinetic Isotope Effects. The ^{13}C, ^{18}O, and ^{2}H kinetic isotope effects in the Cl reaction with HCHO at room temperature are given in Table 4, in which the KIEs calculated with conventional TST and ICVT/SCT are compared to experimental results. The corresponding calculated KIEs in the temperature range of 200−1500 K are available in Tables S2−S6 (Supporting Information). The reaction rate coefficients were obtained by IVTST-M/ISPE and IVTST-M/IOE including the effect of SO coupling. The two models applied for the calculation of the rate coefficients result in a differentiated pattern of the KIEs. For the IOE model the experimental values of the deuterated KIEs, KIE(HCHO/DCDO) and KIE(H^{13}CHO/DCDO), are reproduced well when applying the ICVT/SCT method in combination with scaling of frequencies or only the TST method. The employment of unscaled frequencies lowers the KIEs significantly, resulting in an inverse KIE(HCHO/HCDO). The KIEs, KIE(HCHO/DCDO) and KIE(H^{13}CHO/DCDO), obtained by the ISPE model are significantly higher compared to the IOE model and experimental values. The scaling of frequencies further increases the KIEs. For the KIE(HCHO/HCDO) the calculations with the ISPE model provide values in good agreement with experiment. In comparison to the IOE model, no inverse KIEs are observed for the ISPE model spanning the whole temperature range of 200−1500 K. The same can be said for the TST model without any dual-level corrections (Tables S2−S6). The experimental KIE(H^{12}CHO/H^{13}CHO) can be reproduced by none of the models. All calculations except those applying the ICVT/SCT ISPE model with scaling of the frequencies predict inverse KIEs in the range from 200 to 400 K for the ^{13}C KIE, in contradiction to experimental measurements. For the KIE(HCH^{16}O/HCH^{18}O) only the IOE model predicts KIEs > 1 in admissible agreement with the experimental value.

An investigation of the rate constants for the different isotopologues (Tables S7−S11, Supporting Information) show considerable variational contributions in all models. These contributions are larger for the ISPE model than for the IOE model. Significant tunneling effects are only observed in the low-temperature range (about up to 300 K); they are, however, circumstantial for all isotopologues and models compared to the variational effects. The scaling of frequencies lowers the variational effect resulting in larger KIEs compared to the results

obtained without scaled frequencies. The perdeuterated KIEs of the IOE model with scaled frequencies are in better agreement with experimental values than the same KIEs obtained by the ISPE model. Because the H/D kinetic isotope effect is one of the largest due to the mass ratio of 2, the accuracies of these KIEs are sensitive indicators of the quality of the vibrationally adiabatic ground-state potential energy curve, $V_a^G(s)$. The variational effect is significantly lowered in the DCDO + Cl → DCO + DCl reaction compared to the reaction of Cl with HCHO. In the ISPE model the variational effects are much higher than in the IOE model. The reduction of this effect in the reaction of the perdeuterated species is significantly larger in the ISPE model than in the IOE model, resulting in higher perdeuterated KIEs. The good agreement of the KIE(HCHO/DCDO) for TST in the IOE model is an indication for a low level of variational effects in the reaction system. In the IOE model the vibrationally adiabatic ground-state potential energy curve, $V_a^G(s)$, is affected not only by energy corrections and the scaling of the frequencies but additionally by the corrections of higher-level geometries. In the present case the scaling of frequencies on the higher-level geometry-corrected V_{MEP} results in vibrationally adiabatic ground-state potential energy curves for all isotopologues, which result in improved KIEs compared to unscaled frequenecies. However, the agreement with experiment is not satisfactory for all KIEs. Sellevåg et al.[78] obtained in their study on ^{13}C and deuterium isotope effects in the Cl and OH reaction of CH_4 and CH_3Cl also unsatisfactory results when scaling the Hessians in the ISPE model. We therefore concur with Sellevåg et al.[78] that merely scaling of frequencies is too crude a way of incorporating anharmonicities, and care should be exercised in the interpretation of such results.

To analyze the KIEs in more detail, a factor analysis as described in refs 79 and 80 was performed but limited to investigations of the variational effect and the tunneling contribution only

$$\mathrm{KIE} = \frac{k_{\mathrm{light}}}{k_{\mathrm{heavy}}} = \eta_{\mathrm{trans}}\eta_{\mathrm{rot}}\eta_{\mathrm{vib}}\eta_{\mathrm{tun}}\eta_{\mathrm{var}} \propto \eta_{\mathrm{tun}}\eta_{\mathrm{var}} \qquad (3)$$

The tunneling contribution is given as $\eta_{tun} = \kappa^{SCT}(\mathrm{light})/\kappa^{SCT}(\mathrm{heavy})$, i.e., the ratio of the tunneling factors for the light and the heavy isotopologue; the variational effect is given as $\eta_{var} = \mathrm{KIE}^{ICVT}/\mathrm{KIE}^{TST}$, i.e., the ratio of the KIEs calculated using variational and conventional transition state theory.

Starting with the $^{12}C/^{13}C$ KIE, the factor analysis shows that the variational effect is slightly dominating at low temperatures when using the ISPE model ($\eta_{var}(200\ \mathrm{K}) = 0.98$). For the IOE model the variational and tunneling effects are of almost the same magnitudes; see Table S14, Supporting Information. None of the models predicts the KIE sufficiently large and accurate. Only the ISPE model with scaled frequencies gives KIEs ≥ 1 in the temperature range >250 K. A similar behavior can be found for the $^{16}O/^{18}O$ KIE; the variational effect slightly dominates the KIE in all models (Table S16, Supporting Information). But only calculations based on the IOE model give KIEs > 1 of which the KIE obtained at 298 K, KIE($HCH^{16}O/HCH^{18}O$) = 1.016, compares to the experimental value of 1.08 ± 0.01.[10] For both of the $^{12}C/^{13}C$ and $^{16}O/^{18}O$ KIEs there are no noteworthy tunneling contributions to the KIEs. A large variational effect is found for KIE(HCHO/DCDO) in both models employing unscaled as well as scaled frequencies, viz. $\eta_{var}(200\ \mathrm{K}) = 0.647$ and 0.651 and $\eta_{var}(298\ \mathrm{K}) = 0.767$ and 0.893, respectively, for the IOE model and $\eta_{var}(200\ \mathrm{K}) = 0.649$ and 0.667 and $\eta_{var}(298\ \mathrm{K}) = 0.777$ and 0.893, respectively, for the ISPE model (Table S12, Supporting Information). The calculations show tunneling effects to be of minor importance (Tables S12−S18). However, in all models an unexpected tunneling contribution, $\eta_{tun} < 1$, is observed, especially for the deuterium KIEs (Tables S12 and S13). An inspection of Tables 3 and S7 (Supporting Information) shows that the tunneling contribution, $k^{ICVT}/k^{ICVT/SCT}$, is larger for the C−D abstraction reaction than that for the C−H abstraction reaction and that it increases toward lower temperatures where tunneling becomes more important. Normally one expects tunneling to be more important for the lighter hydrogen than for deuterium. In a low-barrier reaction an isotopic substitution changes the vibrationally adiabatic ground-state potential energy curve, ΔV_a^G, in a relatively drastic way, resulting in different tunneling probabilities. A comparison of the dynamic bottleneck of the reaction for the hydrogen and deuterium reactions shows that at low temperatures (223−400 K) the bottleneck changes from $\zeta = -0.5$ for the hydrogen reaction to $\zeta = -0.1$ for the deuterium reaction for all models applied. This is illustrated for the ISPE model in Figure S2 (Supporting information). Such a drastic shift in the bottleneck position is not observed for the ^{13}C and ^{18}O substituted reactions. The changes in the ΔV_a^G curve and the shifted dynamic bottleneck resulting in a different vibrational force field near the dynamic bottleneck apparently lead to larger tunneling probabilities for the C−D abstraction reaction compared to the C−H abstraction reaction. Obviously, the small curvature tunneling approximation used in the present study is not able to describe the tunneling properly; the "corner cutting effect" for this reaction takes place over a larger part of the reaction swath than the SCT approximation is able to describe.[46,47,81]

4. Discussion

The existence of a barrier along the reaction path—in addition the one resulting from SO coupling in the Cl atom—can be understood from qualitative considerations of MO theory and from our multireference configuration interaction treatment. As outlined in section 3.3. the analyses of the HOMO and the LUMO+1, which are both of A′ symmetry, underline the existence of an avoided crossing in the transition state region. The results of our MRD-CI calculations are in line with these qualitative MO considerations: The leading configuration ($c^2 = 0.87-0.92$) for the A′ state on the reactant side corresponds to 3p AO (Cl), while the leading configuration on the product side ($c^2 = 0.85-0.9$) corresponds to a linear combination involving sp^2 (C) AO. This underlines the existence of an avoided crossing resulting in the barrier to reaction.

Furthermore, the MRD-CI calculations place two electronically excited states, namely, $1^2A''$ and $2^2A'$, considerably low lying at the saddle point. Spin−orbit coupling has a nonnegligible effect on the ground-state PES in the saddle point region. A comparison of the barrier height, $\Delta E^{\ddagger}$, and the energy of the well on the product side, $\Delta E_{\mathrm{post-adduct}}$, (Table 1) at the MP2/aug-cc-pVTZ and MRD-CI/aug-cc-pVTZ//MP2/aug-cc-pVTZ levels of theory shows that the net effect of SO coupling compensates for the incomplete description at the MP2 level compared to the MRD-CI treatment. On the MP2/aug-cc-pVTZ MEP the net effect of SO coupling, i.e., the difference between the SO coupling for reactants and the saddle point, increases the barrier height by 2.7 kJ mol^{-1}. The exit channel, that is, the postreaction adduct and the products, is affected by an increase of 3.3 kJ mol^{-1}. At the RHF-RCCSD(T)/aug-cc-pVTZ level of theory the net effect of SO coupling decreases to 1.4 kJ mol^{-1}

at the saddle point. The present results contrast reports for reactions of chlorine with H_2[76] and HCl,[75] in which the effect of SO coupling is negligible at the saddle point.

Calculations of thermal reaction rate coefficients are, by nature, very sensitive to the precise barrier height of the potential energy surface. This dependency is to a large extent cancelled in the KIE calculations. However, KIEs are sensitive to the shape of the potential energy surface, especially the barrier width and the vibrational force field near the dynamical bottleneck. Because the SO coupling in the Cl atom has little influence on the shape of the barrier[77] the KIEs are much less affected by this than the rate constants. The calculations of KIEs showed that only a variational optimization of the location of the dynamical bottleneck, the position of which differs from one isotopologue to the other, will produce KIEs in reasonable agreement with experiment. Due to the large mass ratios between hydrogen and deuterium, calculations involving these species are particularly affected by the change in the zero-point vibrational energy along the reaction coordinate. IOE dual-level calculations with energy and geometry corrections at a higher level of theory showed how sensitive the KIEs are to changes in the PES and, consequently, to the vibrationally adiabatic ground-state potential energy curve. The variational effects in the rate constants were remarkably reduced compared to the ISPE calculations in which only energy corrections are applied. The scaling of frequencies leads to a reduction of the variational effects in the ICVT/SCT model, resulting in larger KIEs approaching the values obtained by conventional TST. Truhlar and co-workers performed a critical evaluation of dual-level path dynamic methods[42] on three hydrogen-transfer reactions. In their study, the IOE model proved to give more accurate rate constants compared to the results of the ISPE model. However, they did not perform calculations of KIEs.

The tunneling approximation applied—the SCT model—underestimates the real tunneling probability, which is often supposed to be large for heavy−light−heavy hydrogen-transfer reactions with a large reaction path curvature and small skew angles such as in the present reaction. The factor analysis of the KIEs pointed to an inappropriate consideration of tunneling effects, resulting in unexpected tunneling contributions, $\eta_{tun} < 1$.

Studies[82,83] of reactions with barriers to reaction close to zero have indicated that the shift of the generalized transition state from the saddle point ($s = 0$) in the application of canonical variational theory is strongly affected by the partition functions of stretching and bending modes. Consequently, the calculation of accurate reaction rates and KIEs requires an appropriate and correct description of vibrational frequencies along the minimum energy path including anharmonicities. Introducing scaling of the force constants to account for anharmonicity resulted in reaction rate coefficients in good agreement with experiment. The KIE(HCHO/DCDO) was calculated to be in better agreement with experiment for the IOE model whereas the agreement got worse in the ISPE model by introducing this approximation.

For reactions with low barriers, the assumption of a single dividing surface (or bottleneck) becomes invalid for a canonical ensemble. The ICVT model gives a better treatment of this by minimizing the number of vibrational−rotational states at the generalized transition state but only up to the microcanonical variational threshold energy.[84]

Finally, it should be mentioned that the shape of the PES is likely to change with a full multireference configuration interaction treatment of the bond-breaking process, thus affecting the KIEs. However, such a treatment is beyond reach with today's methods and computing facilities.

5. Conclusions

The main results of the present quantum chemistry study of the Cl atom reaction with formaldehyde are:

(a) The hydrogen-transfer reaction is characterized by a minimum energy path on an extremely flat potential surface on the reactant side via a very small barrier—excluding the SO coupling in the Cl atom our best estimate of this barrier is 0.7 kJ mol^{-1} at the MRD-CI/aug-cc-pVTZ//RHF-RCCSD(T)/aug-cc-pVTZ level of theory. Qualitative MO considerations indicate an avoided crossing at the saddle point on the minimum energy path between reactants and products and the demand for a multireference configuration interaction method to calculate the correct barrier height. The MRD-CI calculations place two excited states energetically low lying at the saddle point. Thus, SO coupling is not negligible in the transition state region, resulting in a net increase in the barrier height by only 1.4 kJ mol^{-1} instead of 3.5 kJ mol^{-1} had the SO coupling been negligible at the saddle point.

(b) The calculated reaction rate coefficients based on the MP2/aug-cc-pVTZ minimum energy path with RCCS(T)/aug-cc-pVTZ geometry and MRD-CI/aug-cc-pVTZ//RCCSD(T)/aug-cc-pVTZ energy corrections (IOE model) at the stationary points within the improved canonical variational transition state approximation with small curvature tunneling underestimates the experimental values by factors of 2.9 and 1.4 at 200 and 500 K, respectively. Further, a significant temperature dependency is predicted that is in contrast to experiment. Introducing a scaling of the force constants of all modes yields reaction rates in reasonable agreement with experiment. A factor analysis of the reaction rate coefficients shows almost no tunneling contribution. Consideration of the SO coupling effect results in rate coefficients that are about one-third to one-half lower compared to neglecting SO coupling and fail to reproduce the correct temperature dependency.

(c) Reasonable KIEs are obtained in calculations based on the IOE model with scaled frequencies. The present results are in all cases a considerable improvement compared to the results reported from simple TST calculations by Beukes et al.[9] The employment of scaled frequencies leads to increased KIEs for the two dual-level methods applied in this study. In the ISPE model the perdeuterated KIEs are overestimated. The ^{13}C KIE is correctly predicted >1 at 298 K only by the ISPE model with scaled frequencies. The factor analysis of the KIEs shows unexpected $\eta_{tun} < 1$, suggesting an inappropriate consideration of the tunneling contribution, especially for the H/D KIEs.

Variational transition state theory can explain the observed KIEs to a certain extent. A more sophisticated treatment of anharmonicities and an improved potential energy surface that accounts for the multiconfigurational character of the reaction path will further improve the good results obtained in this study.

Acknowledgment. This work is part of the Atmospheric Chemistry and Transport from Isotopic Analysis project supported by the Norwegian Research Council. The Norwegian Computing Consortium is acknowledged for grants of computing time. Donald G. Truhlar is acknowledged for providing the POLYRATE program. Sigrid D. Peyerimhoff is thanked for providing us a version of the DIESEL-MRD-CI at Innsbruck. M.G.S. acknowledges a grant from the Research Council of Norway through the cultural exchange program between Norway and Austria.

Supporting Information Available: Generalized normal-mode vibrational frequencies as a function of the reaction coordinate, ζ, for the reaction HCHO + Cl → HCO + HCl (Figure S1), vibrationally adiabatic ground-state potential energy curves for the reactions HCHO + Cl → HCO + HCl and DCDO + Cl → DCO + DCl with the position of the bottlenecks of the reactions at 298 K indicated (Figure S2), bond characteristics of reactants and products (Table S1), KIEs in the temperature range of 200−1500 K for KIE(HCHO/DCDO) (Table S2), KIE-(HCHO/HCDO) (Table S3), KIE($H^{12}CHO/H^{13}CHO$) (Table S4), KIE($H^{13}CHO$/DCDO) (Table S5), and KIE($HCH^{16}O/HCH^{18}O$) (Table S6), absolute reaction rate constants and ratios of rate constants for DCDO + Cl (Table S7), DCHO + Cl (Table S8), HCDO + Cl (Table S9), $H^{13}CHO$ + Cl (Table S10), and $HCH^{18}O$ + Cl (Table S11), and factor analysis of the KIE HCHO/DCDO (Table S12), HCHO/HCDO (Table S 13), HCHO/$H^{13}CHO$ (Table S 14), $H^{13}CHO$/DCDO (Table S15), and HCHO/$HCH^{18}O$ (Table S16). This material is available free of charge via the Internet at http://pubs.acs.org.

References and Notes

(1) Niki, H.; Maker, P. D.; Breitenbach, L. P.; Savage, C. M. *Chem. Phys. Lett.* **1978**, *57*, 596.

(2) Fasano, D. M.; Nogar, N. S. *Int. J. Chem. Kinet.* **1981**, *13*, 325.

(3) Poulet, G.; Laverdet, G.; Le Bras, G. *J. Phys. Chem.* **1981**, *85*, 1892.

(4) Foon, R.; Le Bras, G.; Combourieu, J. *C. R. Seances Acad. Sci., Ser. C* **1979**, *288*, 241.

(5) Stief, L. J.; Michael, J. V.; Payne, W. A.; Nava, D. F.; Butler, D. M.; Stolarski, R. S. *Geophys. Res. Lett.* **1978**, *5*, 829.

(6) Michael, J. V.; Nava, D. F.; Payne, W. A.; Stief, L. J. *J. Chem. Phys.* **1979**, *70*, 1147.

(7) Anderson, P. C.; Kurylo, M. J. *J. Phys. Chem.* **1979**, *83*, 2055.

(8) Atkinson, R.; Baulch, D. L.; Cox, R. A.; Hampson, R. F., Jr.; Kerr, J. A.; Rossi, M. J.; Troe, J. *J. Phys. Chem. Ref. Data* **1997**, *26*, 521.

(9) Beukes, J. A.; D'Anna, B.; Bakken, V.; Nielsen, C. J. *Phys. Chem. Chem. Phys.* **2000**, *2*, 4049.

(10) Feilberg, K. L.; Johnson, M. S.; Nielsen, C. J. *J. Phys. Chem. A* **2004**, *108*, 7393.

(11) Dong, F.; Qu, Z.; Zhang, Q.; Kong, F. *Chem. Phys. Lett.* **2003**, *371*, 29.

(12) Møller, C.; Plesset, M. S. *Phys. Rev.* **1934**, *46*, 618.

(13) Pople, J. A.; Seeger, R.; Krishnan, R. *Int. J. Quantum Chem., Quantum Chem. Symp.* **1977**, *11*, 149.

(14) Krishnan, R.; Frisch, M. J.; Pople, J. A. *J. Chem. Phys.* **1980**, *72*, 4244.

(15) Krishnan, R.; Pople, J. A. *Int. J. Quantum Chem.* **1978**, *14*, 91.

(16) Cizek, J. *Adv. Chem. Phys.* **1969**, *14*, 35.

(17) Purvis, G. D., III.; Bartlett, R. J. *J. Chem. Phys.* **1982**, *76*, 1910.

(18) Scuseria, G. E.; Janssen, C. L.; Schaefer, H. F., III. *J. Chem. Phys.* **1988**, *89*, 7382.

(19) Scuseria, G. E.; Schaefer, H. F., III. *J. Chem. Phys.* **1989**, *90*, 3700.

(20) Frisch, M. J.; Trucks, G. W.; Schlegel, H. B.; Scuseria, G. E.; Robb, M. A.; Cheeseman, J. R.; Montgomery, J. A., Jr.; Vreven, T.; Kudin, K. N.; Burant, J. C.; Millam, J. M.; Iyengar, S. S.; Tomasi, J.; Barone, V.; Mennucci, B.; Cossi, M.; Scalmani, G.; Rega, N.; Petersson, G. A.; Nakatsuji, H.; Hada, M.; Ehara, M.; Toyota, K.; Fukuda, R.; Hasegawa, J.; Ishida, M.; Nakajima, T.; Honda, Y.; Kitao, O.; Nakai, H.; Klene, M.; Li, X.; Knox, J. E.; Hratchian, H. P.; Cross, J. B.; Adamo, C.; Jaramillo, J.; Gomperts, R.; Stratmann, R. E.; Yazyev, O.; Austin, A. J.; Cammi, R.; Pomelli, C.; Ochterski, J. W.; Ayala, P. Y.; Morokuma, K.; Voth, G. A.; Salvador, P.; Dannenberg, J. J.; Zakrzewski, V. G.; Dapprich, S.; Daniels, A. D.; Strain, M. C.; Farkas, O.; Malick, D. K.; Rabuck, A. D.; Raghavachari, K.; Foresman, J. B.; Ortiz, J. V.; Cui, Q.; Baboul, A. G.; Clifford, S.; Cioslowski, J.; Stefanov, B. B.; Liu, G.; Liashenko, A.; Piskorz, P.; Komaromi, I.; Martin, R. L.; Fox, D. J.; Keith, T.; Al-Laham, M. A.; Peng, C. Y.; Nanayakkara, A.; Challacombe, M.; Gill, P. M. W.; Johnson, B.; Chen, W.; Wong, M. W.; Gonzalez, C.; Pople, J. A. *Gaussian 03*, revision C.02; Gaussian, Inc.: Wallingford, CT, 2003.

(21) Raghavachari, K.; Trucks, G. W.; Pople, J. A.; Head-Gordon, M. *Chem. Phys. Lett.* **1989**, *157*, 479.

(22) Amos, R. D.; Bernhardsson, A.; Berning, A.; Celani, P.; Cooper, D. L.; Deegan, M. J. O.; Dobbyn, A. J.; Eckert, F.; Hampel, C.; Hetzer, G.; Knowles, P. J.; Korona, T.; Lindh, R.; Lloyd, A. W.; McNicholas, S. J.; Manby, F. R.; Meyer, W.; Mura, M. E.; Nicklass, A.; Palmieri, P.; Pitzer, R.; Rauhut, G.; Schütz, M.; Schumann, U.; Stoll, H.; Stone, A. J.; Tarroni, R.; Thorsteinsson, T.; Werner, H.-J. *MOLPRO, A Package of Ab Initio Programs*, version 2002.6; University College Cardiff Consultants Limited: Cardiff, UK, 2002.

(23) Knowles, P. J.; Hampel, C.; Werner, H. J. *J. Chem. Phys.* **1993**, *99*, 5219.

(24) Knowles, P. J.; Hampel, C.; Werner, H.-J. *J. Chem. Phys.* **2000**, *112*, 3106.

(25) Watts, J. D.; Gauss, J.; Bartlett, R. J. *J. Chem. Phys.* **1993**, *98*, 8718.

(26) Dunning, T. H., Jr. *J. Chem. Phys.* **1989**, *90*, 1007.

(27) Woon, D. E.; Dunning, T. H., Jr. *J. Chem. Phys.* **1993**, *98*, 1358.

(28) Kendall, R. A.; Dunning, T. H., Jr.; Harrison, R. J. *J. Chem. Phys.* **1992**, *96*, 6796.

(29) Peterson, K. A.; Woon, D. E.; Dunning, T. H., Jr. *J. Chem. Phys.* **1994**, *100*, 7410.

(30) Woon, D. E.; Dunning, T. H., Jr. *J. Chem. Phys.* **1995**, *103*, 4572.

(31) Hanrath, M.; Engels, B. *Chem. Phys.* **1997**, *225*, 197.

(32) Muhlhauser, M.; Schnell, M.; Peyerimhoff, S. D. *Mol. Phys.* **2002**, *100*, 2719.

(33) Muhlhauser, M.; Schnell, M.; Peyerimhoff, S. D. *Mol. Phys.* **2002**, *100*, 509.

(34) Gruber-Stadler, M.; Muehlhaeuser, M.; Nielsen, C. J. *J. Phys. Chem. A* **2006**, *110*, 6157.

(35) Buenker, R. J.; Peyerimhoff, S. D. *Theor. Chim. Acta* **1974**, *35*, 33.

(36) Buenker, R. J.; Peyerimhoff, S. D. *Theor. Chim. Acta* **1975**, *39*, 217.

(37) Halkier, A.; Helgaker, T.; Jorgensen, P.; Klopper, W.; Koch, H.; Olsen, J.; Wilson, A. K. *Chem. Phys. Lett.* **1998**, *286*, 243.

(38) Gonzalez, C.; Schlegel, H. B. *J. Chem. Phys.* **1989**, *90*, 2154.

(39) Gonzalez, C.; Schlegel, H. B. *J. Phys. Chem.* **1990**, *94*, 5523.

(40) Corchado, J. C.; Coitino, E. L.; Chuang, Y.-Y.; Fast, P. L.; Truhlar, D. G. *J. Phys. Chem. A* **1998**, *102*, 2424.

(41) Gonzalez-Lafont, A.; Villa, J.; Lluch, J. M.; Bertran, J.; Steckler, R.; Truhlar, D. G. *J. Phys. Chem. A* **1998**, *102*, 3420.

(42) Chuang, Y.-Y.; Corchado, J. C.; Truhlar, D. G. *J. Phys. Chem. A* **1999**, *103*, 1140.

(43) Hu, W. P.; Liu, Y. P.; Truhlar, D. G. *J. Chem. Soc., Faraday Trans.* **1994**, *90*, 1715.

(44) Chuang, Y.-Y.; Truhlar, D. G. *J. Phys. Chem. A* **1997**, *101*, 3808.

(45) Isaacson, A. D.; Sund, M. T.; Rai, S. N.; Truhlar, D. G. *J. Chem. Phys.* **1985**, *82*, 1338.

(46) Truhlar, D. G.; Isaacson, A. D.; Garrett, B. C. Generalized transition state theory. In *The Theory of Chemical Reaction Dynamics*; Baer, M., Ed.; CRC Press: Boca Raton, FL, 1985; Vol. 4; p 65.

(47) Liu, Y.-P.; Lynch, G. C.; Truong, T. N.; Lu, D.-H.; Truhlar, D. C.; Garrett, B. C. *J. Am. Chem. Soc.* **1993**, *115*, 2408.

(48) Garrett, B. C.; Truhlar, D. G.; Grev, R. S.; Magnuson, A. W. *J. Phys. Chem.* **1980**, *84*, 1730.

(49) Fast, P. L.; Corchado, J. C.; Truhlar, D. G. *J. Chem. Phys.* **1998**, *109*, 6237.

(50) Villa, J.; Corchado, J. C.; Gonzalez-Lafont, A.; Lluch, J. M.; Truhlar, D. G. *J. Phys. Chem. A* **1999**, *103*, 5061.

(51) Corchado, J. C.; Chuang, Y.-Y.; Fast, P. L.; Villà, J.; Hu, W.-P.; Liu, Y.-P.; Lynch, G. C.; Nguyen, K. A.; Jackels, C. F.; Melissas, V. S.; Lynch, B. J.; Rossi, I.; Coitiño, E. L.; Fernandez-Ramos, A.; Ellingson, B. A.; Pu, J.; Albu, T. V.; Zheng, J.; Steckler, R.; Garrett, B. C.; Isaacson, A. D.; Truhlar, D. G. *POLYRATE*, version 9.6; University of Minnesota: Minneapolis, MN, 2007.

(52) Ralchenko, Y.; Jou, F.-C.; Kelleher, D. E.; Kramida, A. E.; Musgrove, A.; Reader, J.; Wiese, W. L.; Olsen, K. *NIST Atomic Spectra Database*, version 3.1.2; National Institute of Standards and Technology: Gaithersburg, MD, 2007.

(53) Berning, A.; Schweizer, M.; Werner, H.-J.; Knowles, P. J.; Palmieri, P. *Mol. Phys.* **2000**, *98*, 1823.

(54) *Computational Chemistry Comparison and Benchmark DataBase*; NIST Standard Reference Database 101; National Institute of Standards and Technology: Gaithersburg, MD, 2005.

(55) *Thermodynamic Properties of Individual Substances: Elements Oxygen, Hydrogen (Deuterium, Tritium), Fluorine, Chlorine, Bromine, Iodine, Helium, Neon, Argon, Krypton, Xenon, Radon, Sulfur, Nitrogen, Phosphorus, and Their Compounds, Part 2: Tables*, 4th ed.; Gurvich, L. V., Veyts, I. V., Alcock, C. B., Ed.; Hemisphere Publishing Corp.: New York, 1989; Vol. 1.

(56) Helgaker, T.; Gauss, J.; Joergensen, P.; Olsen, J. *J. Chem. Phys.* **1997**, *106*, 6430.

(57) Bak, K. L.; Jorgensen, P.; Olsen, J.; Helgaker, T.; Klopper, W. *J. Chem. Phys.* **2000**, *112*, 9229.

(58) Dunning, T. H., Jr. *J. Phys. Chem. A* **2000**, *104*, 9062.

(59) Galano, A.; Alvarez-Idaboy, J. R. *J. Comput. Chem.* **2006**, *27*, 1203.

(60) Simon, S.; Duran, M.; Dannenberg, J. J. *J. Chem. Phys.* **1996**, *105*, 11024.

(61) Boys, S. F.; Bernardi, F. *Mol. Phys.* **1970**, *19*, 553.

(62) Kobko, N.; Dannenberg, J. J. *J. Phys. Chem. A* **2001**, *105*, 1944.
(63) Peterson, K. A.; Dunning, T. H., Jr. *J. Chem. Phys.* **1995**, *102*, 2032.
(64) Moule, D. C.; Walsh, A. D. *Chem. Rev.* **1975**, *75*, 67.
(65) Chuang, M. C.; Foltz, M. F.; Moore, C. B. *J. Chem. Phys.* **1987**, *87*, 3855.
(66) Valachovic, L. R.; Tuchler, M. F.; Dulligan, M.; Droz-Georget, T.; Zyrianov, M.; Kolessov, A.; Reisler, H.; Wittig, C. *J. Chem. Phys.* **2000**, *112*, 2752.
(67) Chutjian, A. *J. Chem. Phys.* **1974**, *61*, 4279.
(68) Brand, J. C. D. *J. Chem. Soc.* **1956**, 858.
(69) Bruna, P. J.; Hachey, M. R. J.; Grein, F. *J. Phys. Chem.* **1995**, *99*, 16576.
(70) Harding, L. B.; Goddard, W. A., III. *J. Am. Chem. Soc.* **1977**, *99*, 677.
(71) Ramsay, D. A. *J. Chem. Phys.* **1953**, *21*, 960.
(72) Milligan, D. E.; Jacox, M. E. *J. Chem. Phys.* **1969**, *51*, 277.
(73) Hochanadel, C. J.; Sworski, T. J.; Ogren, P. J. *J. Phys. Chem.* **1980**, *84*, 231.
(74) Bruna, P. J.; Buenker, R. J.; Peyerimhoff, S. D. *J. Mol. Struct.* **1976**, *32*, 217.
(75) Schatz, G. C. *J. Phys. Chem.* **1995**, *99*, 7522.
(76) Capecchi, G.; Werner, H.-J. *Phys. Chem. Chem. Phys.* **2004**, *6*, 4975.
(77) Manthe, U.; Capecchi, G.; Werner, H.-J. *Phys. Chem. Chem. Phys.* **2004**, *6*, 5026.
(78) Sellevåg, S. R.; Nyman, G.; Nielsen, C. J. *J. Phys. Chem. A* **2006**, *110*, 141.
(79) Corchado, J. C.; Truhlar, D. G.; Espinosa-Garcia, J. *J. Chem. Phys.* **2000**, *112*, 9375.
(80) Joseph, T.; Steckler, R.; Truhlar, D. G. *J. Chem. Phys.* **1987**, *87*, 7036.
(81) Skodje, R. T.; Truhlar, D. G.; Garrett, B. C. *J. Phys. Chem.* **1981**, *85*, 3019.
(82) Garrett, B. C.; Truhlar, D. G. *J. Am. Chem. Soc.* **1979**, *101*, 4534.
(83) Garrett, B. C.; Truhlar, D. G. *J. Am. Chem. Soc.* **1979**, *101*, 5207.
(84) Garrett, B. C.; Truhlar, D. G.; Grev, R. S.; Magnuson, A. W. *J. Phys. Chem.* **1980**, *84*, 1730.